C. R. Geoscience 342 (2010) 36–45

Contents lists available at ScienceDirect

Comptes Rendus Geoscience

www.sciencedirect.com

Geomaterials (Ore deposits)

Tectonic implications of new single zircon Pb-Pb evaporation data in the Lossogonoi and Longido ruby-districts, Mozambican metamorphic Belt of north-eastern Tanzania

Implications tectoniques de nouvelles datations Pb-Pb par évaporation sur monozircon dans les districts à rubis de Lossogonoï et de Longido. Ceinture métamorphique mozambicaine du Nord-Est de la Tanzanie

Elisabeth Le Goff [a,*], Yves Deschamps [b], Catherine Guerrot [c]

[a] *Service des ressources minérales, BP 36009, 3, avenue Claude-Guillemin, 45060 Orléans cedex 2, France*
[b] *Areva NC, tour Areva, 1, place Jean-Millier, 92084 La Défense, France*
[c] *Service métrologie, monitoring, analyse, BP 36009, 3, avenue Claude-Guillemin, 45060 Orléans cedex 2, France*

ARTICLE INFO

Article history:
Received 21 October 2008
Accepted after revision 21 September 2009
Available online 3 December 2009

Presented by Zdenek Johan
In memory to Patrice Pinna
(1947–2002).

Keywords:
Mozambique Belt
Tanzania
Ruby
Longido
Lossogonoi
Single zircon Pb-Pb evaporation method

Mots clés :
Chaîne mozambicaine
Tanzanie
Rubis
Longido
Lossogonoï
Méthode d'évaporation Pb-Pb sur monozircon

ABSTRACT

Three single zircon Pb-Pb evaporation dating studies were performed on felsic orthogneisses and migmatites from the Longido and Lossogonoi ruby districts, Mozambique Belt of north-eastern Tanzania, in order to better constrain the geological setting of gemstone mineralizations. Igneous emplacement ages of protoliths ranging between 2636 and 2448 Ma document for the first time the presence of a Neoarchean to Lower Paleoproterozoic (Siderian) basement reworked in the Late Neoproterozoic Mozambique Belt of north-eastern Tanzania. This ancient crust of unknown dimension is well documented farther south, but also in south-eastern Kenya. A shearing event under high-grade amphibolite facies conditions, postdating the Pan-African metamorphic peak at 640 Ma and following nappes emplacement is demonstrated at ca. 610 Ma from metamorphic zircons of Lossogonoi district. In Lossogonoi district, ruby crystallizes during this last stage of deformation.

RÉSUMÉ

Trois datations par la méthode d'évaporation Pb-Pb sur monozircon ont été réalisées sur des orthogneiss et migmatites des districts à rubis de Longido et Lossogonoï, chaîne mozambicaine du Nord-Est de la Tanzanie, afin de mieux contraindre le contexte géologique des minéralisations à gemmes. Les âges de mise en place des protolithes, compris entre 2636 et 2448 Ma, démontrent pour la première fois la présence d'un socle d'âge Néoarchéen à Paléoprotézozoïque inférieur (Sidérien), remanié dans la ceinture mozambicaine tardi-néoprotérozoïque du Nord-Est de la Tanzanie. Cette croûte de dimension inconnue est bien renseignée plus au sud mais aussi dans le Sud-Est du Kenya. Un évènement cisaillant en conditions de faciès amphibolite de haut grade, succédant au pic métamorphique granulitique Panafricain à 640 Ma est mis en évidence vers 610 Ma, à

* Corresponding author.
E-mail address: e.legoff@brgm.fr (E. Le Goff).

1631-0713/$ – see front matter © 2009 Published by Elsevier Masson SAS on behalf of Académie des sciences.
doi:10.1016/j.crte.2009.10.003

partir de zircons métamorphiques du district de Lossogonoï. Dans le district de Lossogonoï, les rubis cristallisent pendant ce dernier épisode de déformation.

1. Introduction

The high-grade terranes of the Mozambique Belt (Holmes, 1951) are part of the East African Orogen (McWilliams, 1981; Stern, 1994) that formed by continent – continent collision of East and West Gondwana fragments during the Late Neoproterozoic, between ca. 640 and 550 Ma (Collins and Pisarevsky, 2005; Key et al., 1989; Meert, 2003). In Tanzania, the Mozambique Belt constitutes a complex imbricated structural unit reworking pro-parte the Archean Tanzanian craton and the Usagaran Paleoproterozoic belt on its eastern border (Fig. 1). During the last decade, numerous field and laboratory studies in geochemistry, geochronology (Möller et al., 2000; Muhongo et al., 1999; Sommer et al., 2003, 2005) as well as updated geological synthesis at belt scale (Dewey and Burke, 1972; Shackelton, 1993; Deschamps et al., 2004; Pinna et al., 2004) have modified and improved the geological knowledge of the Tanzanian Mozambique Belt (Fig. 1). One of the most famous features of the Mozambique belt in Kenya, Tanzania and Madagascar is the occurrence of a wide variety of densely scattered gemstone deposits along the Mozambique Belt (Keller, 1992), earning it the name of the "Gemstone Belt of East Africa" (Knorring and Condliffe, 1987; Malisa and Muhongo, 1990). Recent research based on worldwide reference deposits have enabled a better understanding of the typology of gem deposits (i.e.: primary deposits [igneous, metamorphic, metasomatic, anatectic], secondary deposits [igneous, sedimentary]) and their genetic emplacement processes, specifically for metamorphic-metasomatic processes in amphibolite and low grade granulite facies (Garnier et al., 2004, 2008; Giuliani et al., 2007; Simonet et al., 2008).

However, concerning Tanzania, detailed geological studies allowing a better understanding of the gemstone mineralizations in their geological, structural, metamorphic context at local and regional scale remain scarce (Malisa, 1987; Malisa and Muhongo, 1990; Mercier et al., 1999; Shackelton, 1993; Simonet, 2000). The present work is thus designed to constrain the geological setting of two major ruby deposits of north-eastern Tanzania, through east-west geological cross-sections and geochronological studies in the Masai steppe.

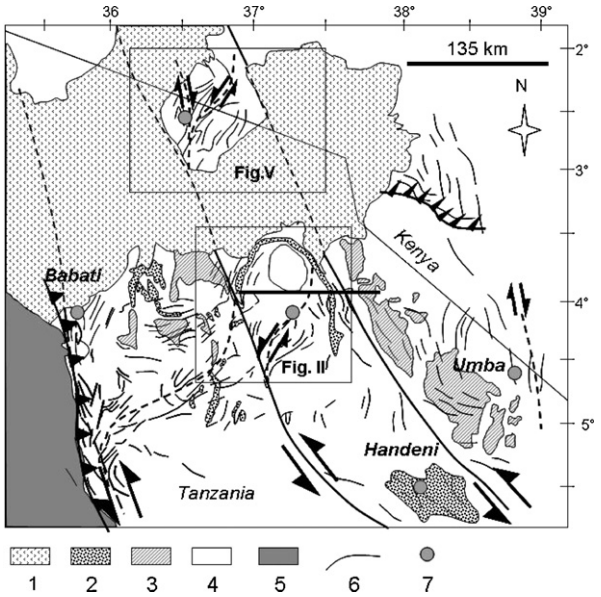

Fig. 1. Simplified geological map of north-eastern Tanzania with location of the studied areas: Fig. V. Longido district. Fig. II. Lossogonoi district. 1. Neogene-Quaternary volcanic formation. 2. Neoproterozoic metasedimentary rocks. 3. Granulitic rocks. 4. Undifferentiated gneisses. 5. Archean gneisses. 6. Foliation pattern. 7. Location of ruby deposits (Lossogonoi, Longido, Handeni, Babati, Umba).

Fig. 1. Carte géologique simplifiée du Nord-Est de la Tanzanie avec la localisation des districts étudiés : Fig. V. Longido. Fig. II. Lossogonoï. 1. Formations volcaniques néogènes et quaternaires. 2. Roches sédimentaires néoprotérozoïques. 3. Granulites. 4. Gneiss indifférenciés. 5. Gneiss archéens. 6. Trajectoire de foliation. 7. Localisation des gisements de rubis (Lossogonoï, Longido, Handeni, Babati, Umba).

2. Analytical methods

Zircons were extracted after crushing ($< 250\,\mu m$) by using standard heavy-liquid and magnetic-separation techniques. Single-zircon dating was carried out using the direct lead evaporation method (Kober, 1986, 1987), according to the detailed technical procedure described by Cocherie et al., 1992. The average $^{207}Pb^*/^{206}Pb^*$ age for all steps is given to $\pm 1\sigma$ standard deviation on all $^{207}Pb^*/^{206}Pb^*$ individual ratios. Where several steps were recorded for a given grain, the "single age" was obtained with a $\pm 1\sigma$ standard deviation calculated with all corresponding recorded $^{207}Pb^*/^{206}Pb^*$ ages. Finally, where several zircons gave the same age (within the analytical uncertainties) over various steps, a weighted average age based on all the individual steps was calculated with $\pm 2\sigma$ (95% confidence limit) using the ISOPLOT/EX program (Ludwig, 1999).

3. The Lossogonoi district

3.1. Geological setting

Despite the occurrence of some of the most famous Tanzanian gemstones producing districts, namely Lossogonoi (ruby), Merelani (tanzanite) and Komolo (tsavorite) (Fig. 2), detailed geological studies in the Masai steppe are scarce (Grainger, 1964; Macfarlane, 1965; Malisa, 1987; Malisa and Muhongo, 1990; Shackelton, 1993). The regional structure is characterized by a large-scale antiform, the Lelatema fold structure, underlined by metasedimentary rocks (quartzites, marbles and pelites). The

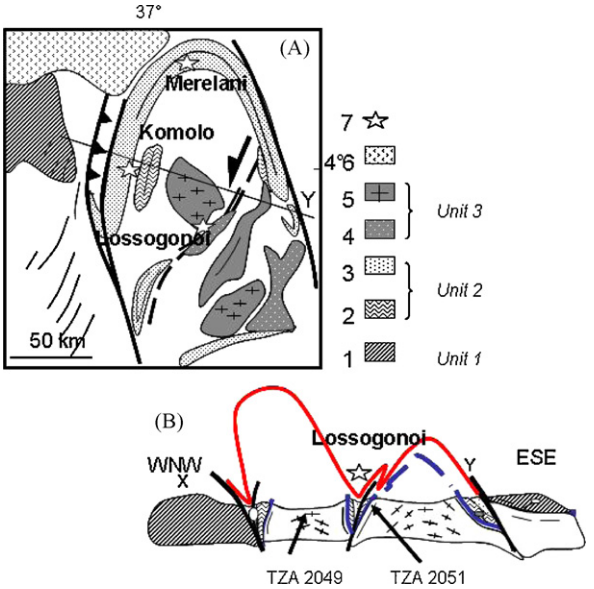

Fig. 2. A. Simplified geological map. **B**. Cross-section of the Lossogonoi district and the Lelatema fold structure in the Masai steppe (Lossogonoi district): 1. Granulitic unit (Loibor Serrit granulite). 2. Migmatitic mafic rocks. 3. Metasedimentary formation. 4. Layered quartzo-feldspathic formation. 5. Layered gneisses and granitic formations, weakly deformed. 6. Cenozoic Rift volcanics. 7. Location of tsavorite deposit (Komolo), tanzanite deposit (Merelani), ruby deposit (Lossogonoi).

Fig. 2. A. Carte géologique simplifiée. B. Coupe de la structure plissée de Lelatema dans la steppe Masai (district de Lossogonoï) : 1. Unité granulitique (granulite de Loibor Serrit). 2. Roches basiques migmatitiques. 3. Formation métasédimentaire. 4. Formation quatzofeldspathique litée. 5. Gneiss lités et granites peu déformés. 6. Volcanites cénozoïques du Rift. 7. Localisation des gîtes à tsavorite (Komolo), tanzanite (Merelani) et rubis (Lossogonoi).

axial plane of the fold trends NNW and dips towards the east. Depending on the authors, this wide structure was produced either during one (Macfarlane, 1965) or two successive superimposed deformational events (Grainger, 1964; Malisa, 1987). Three main structural units are distinguished from west to east (Fig. 2):

– *Unit 1* comprises essentially layered mafic and felsic granulites including some lenses of metasedimentary rocks (marbles, quartzites, graphitic schists), known more to the west as the "Loibor Serrit granulites", belonging to the "Central granulites" defined by Hepworth, 1972. According to Grainger, 1964, this unit is affected by a pervasive north-NNE-trending foliation with a moderate dip towards east-SE. Mafic granulites exhibit a garnet + clinopyroxene + hornblende + plagioclase synkinematic assemblage. Using classical geothermobarometers (Ellis and Green, 1979; Holland and Blundy, 1994; Moecher et al., 1988), P-T conditions of metamorphism are estimated at 12–14 kbar, 700 ± 50 °C (Table 1), thus similar in thermometry but higher in barometry than those obtained in the Usambara and Pare mountains, belonging to the "Eastern granulites" (9–10 kbar, 700–800 °C) (Appel et al., 1998). To the east, at the contact with the metasedimentary unit (unit 2), mafic granulites are retrogressed into mylonitic hornblende ± plagioclase-bearing amphibolites, affected by a gently (20°) south-eastward dipping foliation, trending N20°E. This second deformation event occurs under amphibolite facies metamorphic conditions. The related stretching lineation trends N40°E, with a gently (5°) southwestwards plunge; shear criteria indicate a south-westwards thrusting movement.
– *Unit 2* is a metasedimentary unit made of dolomitic marbles, quarzites, graphitic schists and layered amphibolites with a locally migmatitic aspect. This unit is affected by two deformation events:
  (i) the first one, characterized by a foliation parallel to the layering is coeval with a garnet + kyanite/sillimanite + biotite assemblage observed in metapelites or garnet + kyanite + graphite in graphitic schists;
  (ii) the second one is responsible of the refolding of the whole unit (Lelatema fold) and is associated with vertical shear zones.

Close to the contact with unit one, folded pegmatitic veins are associated with a dextral N20 trending shear zone. In Merelani area, located in the hinge of the Lelatema antiform, P-T conditions have been estimated at 7–9 kbar, 600–720 °C (Malisa, 1987) or 5–6 kbar, 610–670 °C (Maboko and Nakamura, 2002). However, relationships between these estimations and the two deformation events are not clearly established. Further east, in SE Kenya (Taita Hills), P-T conditions in metasedimentary units, which constitute the equivalent of the Masai steppe metasediments, are estimated at 10–12 kbar, 800 °C for D1 and 5–8 kbar, 600–650 °C for D2. The first deformation event is dated at 630–645 Ma (Hauzenberger et al., 2007).
– *Unit 3* outcrops in the central part of the Lelatema fold and comprises essentially strongly deformed biotite or hornblende-bearing quartzo-feldspathic gneisses and weakly deformed granitoids, both constituting the surrounding country rocks of the Lossogonoi ruby-bearing veins (Fig. 2). Indeed, in the central part of the area, near Lossogonoi, granitoids present a N40-trending foliation plan bearing a subhorizontal stretching lineation. Shear bands indicate sinistral movements. These mylonitic shears are marked out by ultramafic bodies clusters, one of them being the host rock of the ruby–bearing Lossogonoi amphibolite ("anyolite") veins (Fig. 2). At the mine scale, a set of four subparallel steeply southward-dipping N60 to N80-trending dark garnet-bearing amphibolite and "anyolite" veins cross-cut a serpentinised and carbonatised meta-peridotite body. Most of the sporadic ruby production since 1968 comes from a single thin (ca. 0.5 m thick) dark-green mineralogically zoned ruby ± garnet amphibolite vein, locally grading to a zoisite-bearing "anyolite" – a local name indicating a rock mainly made up of black hornblende, green zoisite and red corundum (Simonet, 2000). Gem-quality ruby occurs as xenomorphous crystals in occasional pockets, mostly associated to dark green amphibole facies, more rarely with zoisite.

Table 1
Geothermobarometry of garnet-clinopyroxene bearing Loibor Serrit granulites.

Tableau 1
Géothermobarométrie des granulites de Loibor Serrit à grenat et clinopyroxène.

Geothermobarometers after	Sample 2030	Sample 2031
Ellis and Green, 1979 (°C)	620 ± 20	650 ± 40
Holland and Blundy, 1994 (°C)	750 ± 20	820 ± 20
Moecher et al., 1988, at 650–750 °C (kbar)	13–15	12–14

3.2. Geochronology

Single-zircon dating was carried out on two samples of unit 3:

- Sample TZ2049 (3°56.894' S/36°59.213' E) is a widely outcropping weakly deformed pink porphyritic granite. Porphyroclasts of perthitic K-feldspar + plagioclase + - quartz and hornblende are partly recrystallized in a fine-grained granoblastic and synkinematic microcline + plagioclase + quartz + garnet + biotite assemblage. Zircons are numerous, anhedral to sometimes subeuhedral, and of relatively large size (200–500 μm). They are yellow-orange to amber in colour, generally elongated, more or less translucent and frequently present a strong concentric zonation and numerous inclusions. Four zircons selected amongst the most translucent and well-crystallized grains have been analyzed, giving four to seven temperature steps (Table 2). The ages of the first steps are frequently younger than the higher temperature steps (three first steps of zircons A and B). The five steps of zircon C are very homogeneous (2635 Ma) and similar to ages obtained for the last steps of zircon A and the four last steps of zircon B. In contrast, the zircon D is always slightly younger with ages growing with temperature. The mean age, 2636.1 ± 2.4 Ma, calculated on ten temperature steps (Fig. 3) is interpreted as the emplacement age of the granitic protolith (Neoarchean).
- Sample TZ2051 (4°02.816' S/37°07.587' E) belongs to outcrops located close to the ultramafic body hosting the Lossogonoi ruby-mine. These rocks are garnet-biotite-bearing migmatitic gneisses affected by a N115-trending foliation dipping 50° to the southwest. Foliation plane exhibits a N220-trending stretching lineation plunging 40° to the southwest. Some hundred meters farther, similar rocks present a mylonitic texture associated to a subvertical foliation plan, with a lineation pitch of 50° towards the northeast. We interpret the granoblastic plagioclase + microcline + biotite ± garnet assemblage as a synkinematic metamorphic assemblage. Some relics of quartz and perthitic K-feldspar porphyroclasts are however still preserved. The numerous and relatively large (200–500 μm) zircons are classified in two populations:
  (i) the first one consists of elongated crystals with concentric zonations, multifaceted overgrowth on the pyramids, smoky and yellowish-brownish coloured;
  (ii) the second population corresponds to rounded to ovoid zircons, internally homogeneous, translucent and pinkish coloured.

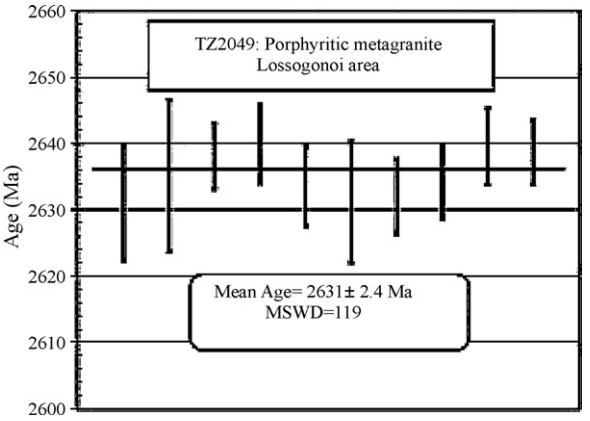

Fig. 3. Diagram of temperature step vs $^{207}Pb/^{206}Pb$ age for the zircons of sample TZ2049, porphyritic metagranite, Lossogonoi area.

Fig. 3. Diagramme de paliers de température vs l'âge de $^{207}Pb/^{206}Pb$ des zircons de l'échantillon TZ2049, métagranite porphyrique, région de Lossogonoï.

Amongst analysed zircons, three of them (A, B, E) belong to the first population and four other translucent crystals (C, D, F, G) belong to the second one.

Elongated zircons of population (i) are characterized by four to eight successive temperature steps (Table 2). The ages of the first steps are frequently younger than high temperature steps, but all ages are old. A "plateau" seems to be reached with the two latest steps of zircons A and B around 2590 Ma. The zircon E is always younger with a maximum age at 2570 Ma.

The ovoid zircons of population (ii) deliver one to eight temperature steps (Table 2). Zircon C, intermediate between rounded and elongated types, indicates more recent ages than elongated zircons, but increasing correlatively with temperature from 700 to 910 Ma. This is interpreted as a recent recrystallisation around an older core. Other zircons (specially D and G) give homogeneous 610 Ma ages on several temperature steps (Table 2).

Two ages are thus obtained:

(i) Neoarchean ages issued from elongated zircons (mean age of 2590.1 ± 4.1 Ma, Fig. 4A) which are interpreted as the protolith age (or minimum protolith age) of the migmatitic gneisses;
(ii) Late Neoproterozoic ages (mean age 609.5 ± 5.6 Ma, Fig. 4B) on 10 steps from two rounded zircons, characterized by low $^{206}Pb/^{208}Pb$ ratios (> 0.03) that are typical for newly formed metamorphic zircons.

These ages are interpretated as representative of the metamorphic recristallization of the layered gneiss, coeval with the zircon neoformation.

Table 2
Isotopic data obtained by lead-evaporation on single-zircon from Tanzania.

Tableau 2
Données isotopiques obtenues par évaporation du plomb sur monozircon de Tanzanie.

Sample	Zircon	T°C	Number of ratios	$^{206}Pb/^{204}Pb$	$^{208}Pb/^{206}Pb$	$^{207}Pb^{*}/^{206}Pb^{*}$ ± 1σ	Step age ± 1σ	Zircon age ± 1σ	Mean age ± 2σ
TZ2049	Zr A	*1420*	*8*	*9740*	*0.076*	*0.17469 ± 141*	*2589.6 ± 13.5*		
Porphyritic metagranite		*1440*	*70*	*16730*	*0.077*	*0.17576 ± 52*	*2608.3 ± 5.0*		
Lossogonoi		*1460*	*68*	*32050*	*0.089*	*0.17694 ± 27*	*2621.8 ± 2.5*		
		1480	19	23310	0.106	0.17812 ± 47	2631.0 ± 4.4		
		1500	72	45520	0.144	0.17870 ± 61	2635.1 ± 5.7	**2634.3 ± 5.7**	
	Zr B	*1400*	*13*	*5110*	*0.113*	*0.17422 ± 115*	*2587.6 ± 11.0*		
		1420	*64*	*37070*	*0.090*	*0.17702 ± 27*	*2622.6 ± 2.5*		
		1440	*72*	*41620*	*0.104*	*0.17694 ± 31*	*2621.5 ± 2.9*		
		1460	72	52920	0.110	0.17867 ± 27	2638.1 ± 2.5		
		1480	54	47160	0.133	0.17892 ± 32	2640.0 ± 3.0		**2636.1 ± 2.4**
		1500	48	71660	0.163	0.17824 ± 32	2633.5 ± 3.0	**2636.0 ± 4.1**	**10 steps**
		1520	51	71540	0.159	0.17815 ± 49	2631.2 ± 4.6		**MSWD = 1.2**
	Zr C	1400	72	88400	0.086	0.17806 ± 30	2632.0 ± 2.8		
		1420	72	55490	0.089	0.17827 ± 29	2634.0 ± 2.8		
		1440	54	46030	0.117	0.17887 ± 31	2639.5 ± 2.9	**2635.3 ± 4.1**	
		1460	31	106040	0.142	0.17873 ± 27	2638.7 ± 2.5		
		1480	*7*	*15120*	*0.095*	*0.17907 ± 76*	*2637.2 ± 7.1*		
	Zr D	*1400*	*12*	*12200*	*0.082*	*0.17571 ± 102*	*2603.1 ± 9.7*		
		1420	*70*	*64320*	*0.108*	*0.17633 ± 72*	*2611.9 ± 6.8*		
		1440	*67*	*88410*	*0.143*	*0.17681 ± 35*	*2619.8 ± 3.3*		
		1460	*62*	*49690*	*0.154*	*0.17719 ± 27*	*2624.2 ± 2.5*		
TZ2051	Zr A	*1400*	*20*	*7930*	*0.065*	*0.15886 ± 83*	*2434.7 ± 8.9*		
Biotite-garnet felsic		*1420*	*69*	*27900*	*0.064*	*0.17081 ± 44*	*2561.3 ± 4.3*		
migmatite Lossogonoi		*1440*	*22*	*20080*	*0.056*	*0.17188 ± 34*	*2572.8 ± 3.3*		
		1460	*14*	*15270*	*0.049*	*0.17242 ± 42*	*2577.2 ± 4.1*		
		1480	55	74430	0.045	0.17362 ± 59	2587.1 ± 5.7		
		1500	59	49180	0.045	0.17360 ± 53	2587.6 ± 5.1	**2587.4 ± 5.4**	
	Zr B	*1400*	*58*	*3560*	*0.090*	*0.12622 ± 234*	*2012.8 ± 33.2*		
Elongated zircons		*1420*	*70*	*12800*	*0.060*	*0.13664 ± 110*	*2171.0 ± 14.1*		
		1440	*72*	*11600*	*0.063*	*0.15130 ± 94*	*2350.0 ± 10.7*		**2590.1 ± 4.1**
		1460	*69*	*25330*	*0.076*	*0.16715 ± 102*	*2519.0 ± 10.3*		**4 steps**
		1480	*71*	*23950*	*0.084*	*0.16835 ± 33*	*2538.1 ± 3.3*		**MSWD = 0.3**
		1500	*67*	*12190*	*0.105*	*0.16866 ± 24*	*2542.0 ± 2.3*		
		1520	66	19550	0.109	0.17384 ± 34	2591.7 ± 3.3	**2591.2 ± 3.7**	
		1540	69	77520	0.096	0.17383 ± 42	2590.8 ± 4.1		
	Zr E	*1400*	*69*	*40300*	*0.055*	*0.16482 ± 48*	*2500.8 ± 4.9*		
		1420	*69*	*68170*	*0.060*	*0.16936 ± 44*	*2547.0 ± 4.3*		
		1440	*40*	*179880*	*0.055*	*0.17165 ± 28*	*2571.0 ± 2.8*		
		1460	*38*	*9140*	*0.066*	*0.17193 ± 31*	*2573.5 ± 3.1*		
	Zr C	*1440*	*30*	*1390*	*0.048*	*0.06452 ± 134*	*714.3 ± 44.3*		
		1460	*67*	*33570*	*0.023*	*0.06261 ± 29*	*685.2 ± 9.8*		
		1480	*57*	*5590*	*0.028*	*0.06667 ± 37*	*815.9 ± 11.5*		
		1500	*63*	*10620*	*0.025*	*0.06775 ± 34*	*850.6 ± 10.4*		
		1520	*66*	*27120*	*0.021*	*0.06896 ± 23*	*890.7 ± 6.8*		
		1540	*31*	*34050*	*0.018*	*0.06970 ± 38*	*908.2 ± 11.3*		
	Zr D	1440	54	26760	0.027	0.06051 ± 33	610.2 ± 11.7		
Round-shape zircons		1460	34	44750	0.026	0.06060 ± 26	615.9 ± 9.2		
		1480	58	84490	0.023	0.06024 ± 19	605.2 ± 7.0		
		1500	68	22130	0.024	0.06044 ± 21	611.6 ± 7.6	**609.8 ± 9.6**	
		1520	61	16140	0.024	0.06038 ± 25	608.2 ± 9.0		
		1540	58	20730	0.023	0.06045 ± 28	609.7 ± 10.0		
	Zr F	*1460*	*6*	*2290*	*0.019*	*0.05944 ± 91*	*549.5 ± 33.7*		
	Zr G	*1420*	*17*	*6470*	*0.020*	*0.05927 ± 42*	*561.6 ± 15.4*		**609.5 ± 5.6**
		1440	*8*	*1680*	*0.034*	*0.05980 ± 61*	*574.1 ± 22.4*		**10 steps**
		1460	27	4670	0.025	0.06034 ± 28	605.9 ± 9.9		**MSWD = 0.1**
		1480	38	5490	0.026	0.06042 ± 24	610.3 ± 8.5		
		1500	65	12920	0.020	0.06050 ± 28	611.6 ± 9.9	**609.5 ± 10.4**	
		1520	61	8380	0.021	0.06045 ± 32	608.2 ± 11.6		
		1540	*8*	*1950*	*0.039*	*0.06062 ± 26*	*616.5 ± 9.3*		
		1560	*8*	*5580*	*0.020*	*0.06047 ± 26*	*611.1 ± 9.2*		
TZ2035	Zr A	*1400*	*40*	*5630*	*0.110*	*0.14710 ± 79*	*2303.1 ± 9.3*		
Garnet-bearing felsic		*1420*	*71*	*22490*	*0.111*	*0.15255 ± 32*	*2371.2 ± 3.6*		
orthogneiss		*1440*	*68*	*14180*	*0.116*	*0.15333 ± 29*	*2380.1 ± 3.2*		
		1460	60	14230	0.138	0.16090 ± 113	2453.2 ± 11.9		
		1480	46	13830	0.140	0.16045 ± 43	2455.9 ± 4.5	**2454.4 ± 9.5**	

Table 2 (*Continued*)

Sample	Zircon	T°C	Number of ratios	$^{206}Pb/^{204}Pb$	$^{208}Pb/^{206}Pb$	$^{207}Pb^*/^{206}Pb^*$ ± 1σ	Step age ± 1σ	Zircon age ± 1σ	Mean age ± 2σ
Longido	Zr B	*1400*	*60*	*8690*	*0.102*	*0.13959 ± 209*	*2196.0 ± 26.2*		
		1420	*39*	*16290*	*0.103*	*0.14177 ± 196*	*2224.8 ± 24.1*		
		1440	*64*	*21940*	*0.115*	*0.15469 ± 82*	*2389.4 ± 9.0*		
		1460	*18*	*24650*	*0.120*	*0.15655 ± 111*	*2406.7 ± 12.1*		
		1480	*66*	*7610*	*0.123*	*0.15791 ± 56*	*2427.4 ± 6.0*		
		1500	13	26800	0.128	0.16041 ± 115	2447.8 ± 12.2		**2447.8 ± 4.4**
		1520	54	53580	0.127	0.15979 ± 63	2446.8 ± 6.7	**2446.0 ± 6.9**	**9 steps**
		1540	54	41000	0.124	0.15943 ± 46	2444.8 ± 4.9		**MSWD = 0.7**
	Zr C	*1400*	*31*	*2180*	*0.077*	*0.09516 ± 89*	*1513.6 ± 17.7*		
		1420	*61*	*4010*	*0.088*	*0.11543 ± 196*	*1855.7 ± 30.9*		
		1440	*68*	*6080*	*0.101*	*0.14076 ± 78*	*2226.9 ± 9.6*		
		1460	*70*	*10070*	*0.119*	*0.15395 ± 63*	*2383.2 ± 7.0*		
		1480	*68*	*21070*	*0.121*	*0.15742 ± 66*	*2421.0 ± 7.2*		
		1500	*69*	*21610*	*0.124*	*0.15688 ± 59*	*2415.9 ± 6.4*		
		1520	40	6070	0.123	0.15910 ± 43	2441.5 ± 4.5		
		1540	62	7170	0.128	0.16041 ± 95	2450.0 ± 10.0	**2446.5 ± 9.4**	
	Zr D	*1400*	*39*	*4000*	*0.108*	*0.13753 ± 116*	*2181.6 ± 14.8*		
		1420	*7*	*6350*	*0.107*	*0.14772 ± 85*	*2309.7 ± 10.0*		
		1440	*7*	*8320*	*0.118*	*0.15606 ± 70*	*2405.8 ± 7.7*		
		1460	27	25980	0.124	0.16036 ± 105	2448.3 ± 11.0		
		1480	20	12950	0.124	0.16033 ± 107	2447.8 ± 11.3	**2448.09 ± 11.2**	

Errors on step age and on zircon age are equal to the standard deviation (1σ level), taken into account all individual $^{207}Pb^*/^{206}Pb^*$ ratios. The weighted average age is based on $^{207}Pb^*/^{206}Pb^*$ step ages at 2σ (95% confidence limit). Steps in italic are not considered in the zircon age and average age.
Les erreurs des âges sur les paliers et zircons sont équivalents à la déviation standard (1σ level), en prenant en compte tous les rapports $^{207}Pb^*/^{206}Pb^*$. L'âge moyen pondéré est basé sur les âges des paliers $^{207}Pb^*/^{206}Pb^*$ à 2σ (95 % limite de confiance). Les paliers en italiques ne sont pas pris en compte dans l'âge des zircons et l'âge moyen.

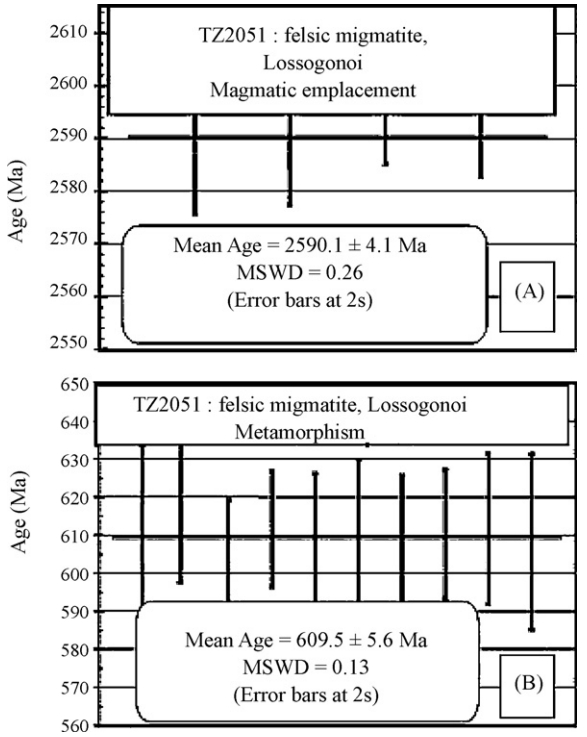

Fig. 4. Diagram of temperature step vs $^{207}Pb/^{206}Pb$ age for the zircons of samples TZ2051, biotite-garnet felsic migmatite, Lossogonoi area. A. Elongated and zoned magmatic zircons. B. Multifaceted and round-shaped metamorphic zircons.

Fig. 4. Diagramme de paliers de température vs l'âge de $^{207}Pb/^{206}Pb$ des zircons de l'échantillon TZ2051, migmatite feldspathique à biotite grenat. A. Zircons magmatiques allongés et zonés. B. Zircons métamorphiques arrondis et multifacettés.

Two events are thus defined: a Neoarchean magmatic event at ≥ 2590.1 ± 4.1 Ma and a Late Neoproterozoic (Pan-african) metamorphic event at 609.5 ± 5.6 Ma, which also corresponds to the age of ruby formation (see discussion).

4. The Longido district

The Longido district (Fig. 1V) correspond to a cluster of ruby-bearing "anyolite" occurrences (Guest and Pickering, 1966; Hartley, 1965) hosted in typically small serpentinized ultramafic bodies scattered within high-grade metamorphic and migmatitic rocks of the Mozambique Belt. Metasediments are dominant, including pelitic and psammitic compositions (quartzo-feldspathic gneisses), aluminous terms (biotite-kyanite-garnet gneisses), quartzitic layers and local thin marble bands. Hornblende-gneisses and amphibolites layers are less common (Guest and Pickering, 1966; Hartley, 1965). Foliation with a dominant NNE-SSW trend and a nearly subvertical dip is associated with large-scale isoclinal folds plunging at shallow angles to the ENE or northeast and sinistral and dextral shear zones, where ultramafic bodies hosting ruby-veins are preferentially hosted. A later folding event associated to open folds is evidenced by complex patterns of metamorphic foliation at map and outcrop scale (Fig. 5).

Detailed study of mineralisation and its geological environment was focused on the main current ruby-producing site, namely the Mundarara underground mine ($X = 36°\ 28.421'E$; $Y = 2°\ 37.876'S$) and the very close artisanal Mula mine, of similar geological characteristics ($36°\ 28.219'\ E$; $2°\ 38.014'S$) (Fig. 6). Ruby ore ("anyolite") occurs in both mines as single foliated and transversally zoned "veins" – actually very flat (< 1 m thick for ca. 150 to 250 m lateral extension and down dip in the Mundarara mine) pinch and swell lenses – boudinaged in the regional

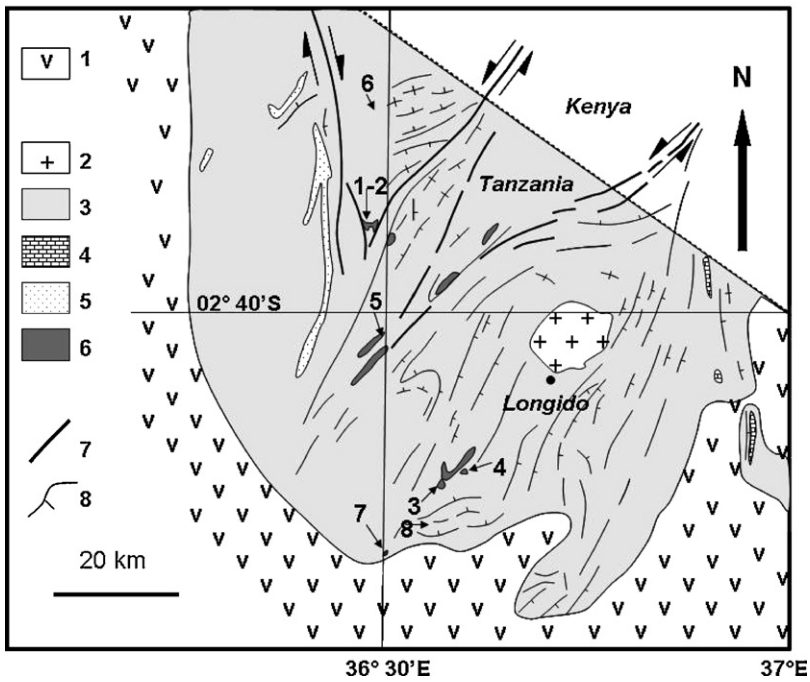

Fig. 5. Simplified geological map of Longido area and location of ruby-deposits. Legend of the geological map: 1-Neogene Rift volcanics. 2–6. Neoproterozoic Mozambique Belt: 2. Late Pan-African granite. 3. Undifferentiated gneiss. 4. Marble. 5. Quartzite. 6. Serpentinite. Structural elements: 7. Fault with kinematics. 8. Foliation pattern. "Anyolite" occurrences: 1. Mundarara mine. 2. Mula mine. 3. Lomwinyi. 4. Elkunulesilali. 5. Ketumbeine. 6. Engare Naibor. 7. Lolkinyoyo. 8. Kimasarua.

Fig. 5. Carte géologique simplifiée de la région de Longido et localisation des gîtes à rubis. Légende de la carte géologique :1. Volcanites néogènes du Rift. 2–6. Ceinture néoprotérozoïque de Mozambique: 2. Granite tardipanafrican. 3. Gneiss indifférenciés. 4. Marbres. 5. Quartzite. 6. Serpentinite. Eléments structuraux : 7. Faille avec cinématique. 8. Trajectoires de la foliation. Indices d'« anyolite » : 1. Mine de Mundarara. 2. Mine de Mula. 3. Lomwinyi. 4. Elkunulesilali. 5. Ketumbeine. 6. Engare Naibor. 7. Lolkinyoyo. 8. Kimasarua.

metamorphic foliation. Field and thin section structural arguments bring to interpret "anyolite" emplacement and ruby crystallisation as the result of synmetamorphic – metasomatic processes in an open system.

Local structure involves several lithotectonic units separated by steeply-dipping north-south to NNE-SSW syn-metamorphic ductile strike-slip shear faults (Fig. 6). A highly-deformed serpentinized ultramafic body of harzburgitic origin (Ketto, 2008; Simonet, 2000), host of the ruby-bearing anyolite veins, geometrically overlain by coarse-grained massive to foliated orthoamphibolites constitute the central ultramafic-mafic units (2 and 4, Fig. 6). Synkinematic garnet + plagioclase + hornblende ± quartz, garnet + clinopyroxene + plagioclase + hornblende + quartz or clinopyroxene + plagioclase + hornblende + quartz assemblages in metabasites bring to P-T conditions of deformation of 12–13 kbar and 670–720 °C (Ketto, 2008). A narrow and discontinuous submeridian tectonic slice (unit 3, Fig. 6) of banded leucocratic orthogneiss is intercalated between the ultramafic – mafic units 2 and 4. The contact is clearly identified as a major subvertical sinistral-normal shear fault. Both sides of the mafic-ultramafic units are metasedimentary units, made of dominant aluminous biotite-garnet ± kyanite migmatitic paragneiss, leucocratic quartzo-feldspathic gneiss, calc-silicate clinopyroxene gneiss layers, amphibolite layers and thin impure marble levels, corresponding to the regional metasedimentary series of Guest and Pickering, 1966; Hartley, 1965. The syn-metamorphic dextral shear-fault nature of both contacts between metasedimentary and ultramafic-mafic units is evidenced by the mylonitic character of paragneisses foliation and clear dextral shear criteria. Close to the contact, mylonitic metapelitic rocks are retrogressed in a biotite-bearing synkinematic assemblage. Late post-foliation north-south to NW-SE trending upright open folds with subhorizontal axis affect all units at different scales, inducing medium-to-large-scale perturbations of the metamorphic foliation pattern (Fig. 6).

4.1. Geochronology

Sample TZ2035B ($X = 36^\circ\ 28.593'$ E/$Y = 02^\circ\ 37.891'$ S) is a garnet-bearing felsic orthogneiss representative of unit 3 (Fig. 6). The orthogneiss exhibits a centimetre-scale alternance of hornblende + plagioclase + quartz ± clinopyr-clinopyroxene, hornblende + plagioclase + garnet + quartz and garnet + hornblende + K-feldspar + quartz layers. Garnet is never in contact with clinopyroxene.

Zircons are rather big (300–800 μm), slightly pinkish to smoky, elongated, sometimes subeuhedral, and generally translucent. They contain numerous opaque inclusions, numerous cavities, and are frequently fissured. Pyramids very often exhibit multifaceted overgrowths. Four crystals have been analysed, each one delivering from five to eight

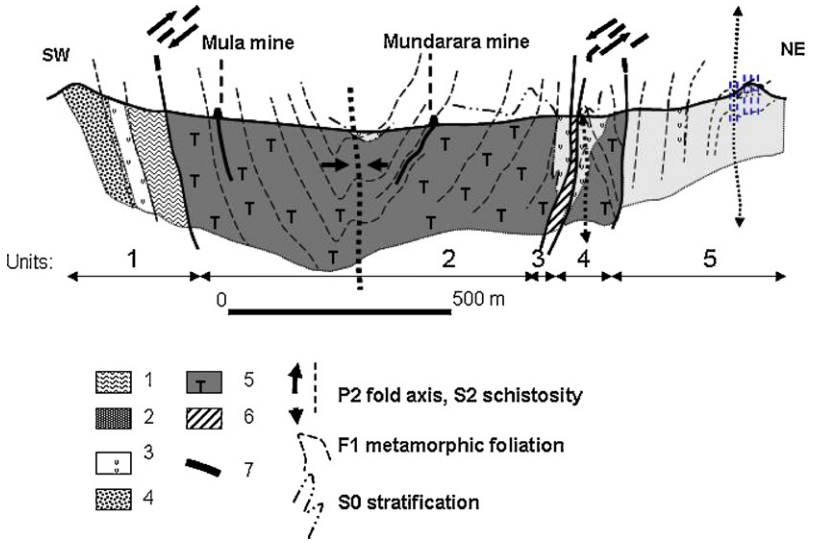

Fig. 6. Geological cross-section of Mula and Mundarara mines in Longido district. 1: Migmatic paragneiss (biotite + garnite ± kyanite); 2: marble lens; 3: amphibolite, calc-silicate gneiss; 4: quartzo-feldspathic gneiss; 5: serpentinite; 6: orthogneiss; 7: anyolite vein.

Fig. 6. Coupe géologique des mines à rubis de Mula et Mundarara dans le district de Longido. 1 : paragneiss migmatique à biotite + granat ± disthène ; 2 : marbre ; 3 : amphibolite, gneiss calco-silicaté ; 4 : gneiss quartzofeldspathique ; 5 : serpentinite ; 6 : orthogneiss ; 7 : veine d'anyolite.

temperature steps. The resulting ages are reported in Table 2. On all of these zircons, an increase of age is correlated with an increase of temperature, with a maximum range between 1510 and 2450 Ma for zircon C. This reveal important lead losses, either linked to very high uranium content and thus an important deterioration of the crystal lattice during disintegrations, or related to a major metamorphic event. The non-metamict character of zircons, as well as the presence of important overgrowths, favour the second assumption, the metamorphism being able to induce a partial recrystallization of grains and thus episodical lead losses. Age of this event is not constrained. High temperature steps (Table 2) on all crystals are nevertheless homogeneous and several steps on a single zircon grain correspond to a same age at around 2450 Ma. This is confirmed on the two last steps of zircons A, C and D, as well as on the three last steps of zircon B. We thus reach a repetitive plateau on several steps and several zircon grains, which can be considered as representative of the crystallization age of this orthogneiss. The mean weighted age calculated on nine steps (Fig. 7) of 2447.8 ± 4.4 Ma is interpreted as the emplacement age of the orthogneiss protolith (Lower Paleoproterozoic or Siderian).

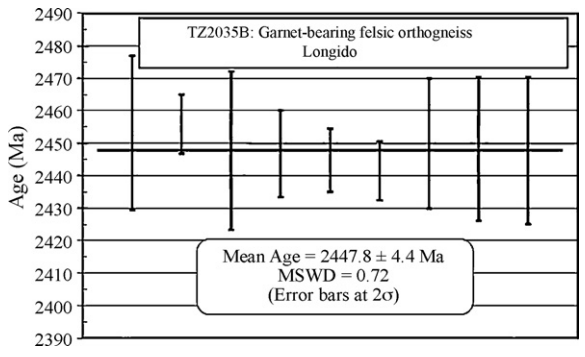

Fig. 7. Weighted mean of different $^{207}Pb^{*}/^{206}Pb^{*}$ ages for retained steps of zircons from sample TZ2035, garnet-bearing felsic orthogneiss, Mundarara mine, Longido.

Fig. 7. Moyenne pondérée des différents âges $^{207}Pb^{*}/^{206}Pb^{*}$ pour les paliers retenus de l'échantillon TZ2035, orthogneiss acide à grenat, mine de Mundarara, Longido.

5. Discussion and conclusion

5.1. Lossogonoi area

Structural relationships between the dated Archean gneisses (this study) and other units in the Masai steppe are poorly documented. According to our field observations, Archean gneisses are overthrusted by metasedimentary units (marbles, quartzites, pelites) – assumed to be of neoproterozoic age, see below – and the Loibor Serrit granulites (units 1 and 2). Both should have been affected by the 640 Ma granulitic metamorphism, if we assume the equivalence between the Masai and Umba steppe metasediments and the Loibor Serrit and Eastern granulites (Pare and Usambara mountains). This hypothesis remains open to verification. Due to the lack of outcrops, the contact between Archean rocks and Neoproterozoic metamorphic units is not observed. Nevertheless, occurrence of granulitic assemblages in Archean gneisses would be a crucial argument to understand initial relationships between Archean and Neoproterozoic units. At the present day, no such assemblage has been observed, but in fact this could be partly due to unfavourable granitic to granodioritic whole-rock compositions. The strong heterogeneity of deformation in the Archean gneisses in comparison with the overlying Neoproterozoic units is also another point to be underlined. Indeed, the sub-isotropic granite

dated at 2636.1 ± 2.4 Ma (TZ2049) does not show any younger ages that could be related to a later metamorphic event. In contrast, the mylonitic layered gneisses dated at 2590.1 ± 4.1 Ma, located at the vicinity of a strongly ductile lithology (i.e. serpentinites) reveal a metamorphic recrystallization episode at 610 Ma. In both lithologies, no evidence of the 640 Ma episode of recrystallization is observed. We thus consider that Archean units constitute an old (autochtonous or para-autochtonous?) basement, non-affected by the 640 Ma-old peak granulitic event. Thrusting of Neoproterozoic granulitic nappes, responsible of the exhumation of high-pressure units occurred thus after the peak of granulitic metamorphism dated at 640 Ma, in amphibolite facies conditions. The stacked units were later affected by folding and shearing in amphibolite facies at 610 Ma, during the final shortening event. The 610 Ma shearing deformation event seems to be coeval with the crystallization of ruby in Lossogonoi area. Indeed, shear zones affect both host-rocks and are consistent with deformation and syn-tectonic mineralogical assemblages observed in ruby-bearing veins.

5.2. Longido area

The complex imbrications of lithotectonic units resulting from the Pan-African thrusting, folding and shearing tectonics make difficult the reconstruction of the original succession. A first deformation event is characterized by a pervasive foliation, meanwhile a second one is related to local subvertical shear zones. Two distinct lithostratigraphic packages are evidenced:

(i) a volcano-sedimentary succession affected by the two deformational events, grading from ultramafic-mafic terms at the bottom towards supracrustals sedimentary argillaceous and detrital sequences. Synkinematic assemblages lead to P-T conditions of D1 deformation in metabasites of 12–13 kbar and 670–720 °C (Ketto, 2008). In aluminous metapelites, this event is expressed by a garnet + kyanite + biotite assemblage, which is retrogressed in biotite-muscovite mylonitic gneiss in D2 shear zone. By comparison with other domains of the Mozambique Belt, this succession is correlated with the Neoproterozoic sequences identified in the upper allochtonous granulitic nappes of the Western granulites and Eastern granulites, (Hauzenberger et al., 2007), as well as in the Mahenge and Morogoro districts (Le Goff et al., 2008), were a maximum age of sedimentation for these platform metasedimentary series was recently constrained at 686 ± 7 Ma by electronic microprobe U-Pb-Th datation (Le Goff et al., 2008).

(ii) a Lower Proterozoic orthogneissic unit (protolith age 2447 Ma, this study), interpreted as a basement unit slice, exhumated and structurally reworked during the Pan-African tectonometamorphic event. This unit is thus to be correlated with the lower autochtonous or para-autochtonous basement domain of the Mozambique Belt, where extensive occurrences of tonalitic – trondhjemitic and granitic gneisses of Neoarchean (Johnson et al., 2003; Maboko, 1995; Möller et al., 1998; Muhongo et al., 2001; Sommer et al., 2003, 2005), and Paleoproterozoic (Cutten and Johnson, 2006) emplacement ages are well documented.

5.3. Conclusions

This study improves the regional geological knowledge of the Mozambique belt in the north-eastern part of Tanzania and documents for the first time in this area the existence of Archean (2.63 and 2.59 Ga in Lossogonoi) and Paleoproterozoic (2.45 Ga in Longido area) relics reworked during the Pan-African tectono-metamorphic event in this part of the belt. Such an ancient crust has already been evidenced further south in the Magobike region, where SHRIMP U-Pb dating on zircon reveal an Archean (2.7 Ga) age for granitic protoliths (Johnson et al., 2003). Furthermore, several Late Archean Pb-Pb evaporation and SHRIMP U-Pb ages are known on high-grade gneisses from the Mozambique Belt of eastern Tanzania (igneous emplacement ages ranging between 2740 and 2608 Ma) (Muhongo et al., 2001) and 2648 Ma (Sommer et al., 2003). More recently, in the SE Kenya, east of the Galana shear zone, 1500 to 2900 Ma Nd model ages were obtained in migmatitic gneisses (Hauzenberger et al., 2007).

According to our structural and geochronological data, we consider that both Neoproterozoic volcano-plutonic and metasedimentary formations are affected by a first deformation event under high-pressure granulitic conditions at 640 Ma. These stacked units are later thrusted over an old Neoarchean to Lower Paleoproterozoic basement during a second deformation event, under amphibolite facies conditions. Finally all these units are sheared and folded at 610 Ma. During this last stage, deformation is strongly heterogeneous and is characterized by shear zones following highly ductile zone such serpentinites bodies where are located ruby veins at Longido and Lossogonoi districts. In both districts, ruby is coeval with this deformation event. Furthermore, chemical and mineralogical zonations between the ruby vein and the country rocks indicate that a metamorphic-metasomatic process is responsible of the crystallization of ruby as already suggested (Simonet, 2000). Datation of ruby veins (anyolite) has not been investigated. However, in Lossogonoi district, geochronological data on migmatitic gneiss affected by this episode indicate an age of 610 Ma that we interpret as the age of the shear zone and consequently the age of cristallization of ruby.

References

Appel, P., Möller, A., Schenk, V., 1998. High-pressure granulite facies metamorphism in the Pan-African belt of eastern Tanzania: P-T-t evidence against granulite formation by continent collision. J. Metab. Geol. 16, 491–509.

Cocherie, A., Guerrot, C., Rossi, P., 1992. Single-zircon dating by step-wise Pb evaporation: Comparison with other geochronological techniques applied to the Hercynian granites of Corsica, France. Chem. Geol. 101, 131–141.

Collins, A.S., Pisarevsky, S.A., 2005. Amalgamating eastern Gondwana: The evolution of the Circum-Indian Orogens. Earth Sci. Rev. 71, 229–270.

Cutten, H.N.C., Johnson, S.P., 2006. Tectonic evolution of the Mozambique Belt, Eastern Africa. In: 21st Colloquium of African Geology. Maputo, Mozambique, 3–5 July, Abstracts volume, pp. 33–34.

Deschamps, Y., Milesi, J.P., Muhongo, S., Kampunzu†, A.B., Le Goff, E., Pinna†, P., Simonet, C., Duguey, E., Marot, A., Guillou, Y., Pouradier, A.,

Ralay, F., Heinry, C., Chene, F., Mcharo, B.A., Joannès, C., 2004. Géologie et Minéralisations à gemmes d'Afrique de l'Est/Geology and Gemstone Deposits of East Africa, scale 1:4,000,000. In: 20th Colloquium of African Geology. Orléans, France, 2–7 June, Abstracts volume, p. 134.

Dewey, J.F., Burke, K., 1972. Orogeny in Africa. In: Dessauvagie, T.F.J., Whiteman, A.J. (Eds.), Orogeny in Africa. Department of Geology, University of Ibadan, Ibadan, pp. 583–608.

Ellis, D.J., Green, D.H., 1979. An experimental study of Ca upon garnet – clinopyroxene Fe-Mg exchange. Contrib. Miner. Petrol. 71, 13–22.

Garnier, V., Giuliani, G., Ohnenstetter, D., Fallick, A.E., Dubessy, J., Banks, D., Hoàng Quang, V., Lhomme, Th., Maluski, H., Pêcher, A., Bakhhsh, K.A., Pham Van, L., Schwarz, D., 2008. Marble hosted ruby deposits from central and South-East Asia: towards a new genetic model. Ore. Geol. Rev. 34, 169–191.

Garnier, V., Giuliani, G., Ohnenstetter, D., Schwarz, D., 2004. Les gisements de corindon : classification et genèse. Regn. Miner. 55, 7–35.

Giuliani, G., Ohnenstetter, D., Garnier, V., Fallick, A.E., Rakotondrazafy, M., Schwarz, D., 2007. The geology and genesis of gem corundum deposits. In: Raeside, ER (Ed.), Geology of gem deposits. Mineralogical Association of Canada, Short course Series, 37. Yellowknife, Canada, pp. 23–78.

Grainger, D.J., 1964. Geological map at 1:125,000, Shambaraï, no. 71, Tanzanian Geological Survey.

Guest, N.J., Pickering R., 1966. Quarter Degree Sheet 40 Gelai & Ketumbeine, Scale 1:125,000, First edition, Guest, N.J., 1949–50, revised with additions by Pickering, R., 1963. Published by the Mineral Resources Division, Dodoma. Ministry of Industries, Mineral Resources and Power.

Hartley, E.W., 1965. Quarter Degree Sheet 41 Longido Scale 1:125,000, First edition, Hartley, E.W., 1963, including previous work by Guest, N.J., 1949 and 1951, compiled, drawn and published by Geological Survey Division, Dodoma. Ministry of Industries, Mineral Resources and Power.

Hauzenberger, C.A., Sommer, H., Fritz, H., Bauernhofer, A., Kröner, A., Hoinkes, G., Wallbrecher, E., Thöni, M., 2007. SHRIMP U-Pb zircon and Sm-Nd garnet ages from the granulite-facies basement of SE Kenya: evidence for Neoproterozoic polycyclic assembly of the Mozambique Belt. J. Geol. Soc. London 164, 189–201.

Hepworth, J.V., 1972. The Mozambique orogenic belt and its foreland in Northeast Tanzania: a photogeologically based study. J. Geol. Soc. London 128 (Part 5), 461–500.

Holland, T., Blundy, J., 1994. Non-ideal interaction in calcic amphiboles and their bearing on amphibole-plagioclase thermometer. Contrib. Miner. Petrol. 6 (4), 433–447.

Holmes, A., 1951. The sequence of Precambrian orogenic belts in South and Central Africa. In: Sandford, K.S., Bondel, F. (Eds.), 18th International Geological Congress, Association of African Geological Surveys, London, 254–269.

Johnson, S.P., Cutten, H.N.C., Muhongo, S., De Waele, B., 2003. Neoarchean magmatism and metamorphism of the western granulites in the central domain of the Mozambique Belt, Tanzania; U/Pb SHRIMP geochronology and P-T estimates. Tectonophysics 375 (1–4), 125–145.

Keller, P.C., 1992. Gemstones of East Africa. Geoscience Press, USA Tucson, 160 p.

Key, R.M., Charsley, T.J., Hackman, B.D., Wilkinson, A.F., Rundle, C.C., 1989. Superimposed upper Proterozoic collision-controlled orogenies in the Mozambique orogenic belt of Kenya. Precambr. Res. 44, 197–225.

Ketto D., 2008. Geological investigation of Longido ruby deposit, North-Eastern Tanzania. Master in Science (Geology) University of Dar Es Salaam.

Knorring, O., Condliffe, E., 1987. Mineralized pegmatites in Africa. Geol. J. 22, 253–270.

Kober, B., 1986. Whole grain evaporation for $^{207}Pb/^{206}Pb$–age investigations on single zircons using a double filament thermal ion source. Contrib. Miner. Petrol. 93, 482–490.

Kober, B., 1987. Single-zircon evaporation combined with Pb+ emitter bedding for $^{207}Pb/^{206}Pb$-age investigations using thermal ion mass spectrometry, and implications for zirconology. Contrib. Miner. Petrol. 96, 63–71.

Le Goff E., Deschamps, Y., Guerrot C., Cocherie A., Milesi, J.P., Ketto, D., Malisa, E., Muhongo, S., 2008. New geochronological data by single zircon Pb-Pb evaporation method in north-eastern Tanzania: regional implications for the Tanzanian Mozambique belt and gemstones mineralization. 33rd IGC Oslo, 2008, August 6–14.

Ludwig, K.R., 1999. Isoplot/Ex version 2.06: A Geochronological Toolkit for Microsoft Excel. Berkeley Geochronology Center, Special Publication 1a. 49 p.

Maboko, M.A.H., 1995. Neodymium isotopic constraints on the protoliths ages of rocks involved in Pan-african tectonism in the Mozambique Belt of Tanzania. J. Geol. Soc. London 152, 911–916.

Maboko, M.A.H., Nakamura, E., 2002. Isotopic dating of Neoproterozoic crustal growth in the Usambara Mountains of Northeastern Tanzania: evidence for coeval crust formation in the Mozambique Belt and the Arabian-Nubian Shield. Precambr. Res. 113, 227–242.

Malisa, E., 1987. Geology of the tanzanite gemstone deposits in the Lelatema area, NE Tanzania, Annales Academiae Scientiarum Fennicae, series A, 146.

Malisa, E., Muhongo, S., 1990. Tectonic setting of gemstone mineralization in the Proterozoic metamorphic terrane of the Mozambique belt in Tanzania. Precambr. Res. 46, 167–176.

Macfarlane A,, 1965. Geological map at 1:125,000, Arusha Chini, no. 72, Tanzanian Geological Survey.

McWilliams, M.O., 1981. Paleomagnetism and Precambrian tectonic evolution of Gondwana. In: Kröner, A. (Ed.), Precambrian Plate Tectonics. Elsevier, Amsterdam, pp. 649–687.

Meert, J.G., 2003. A synopsis of events related to the assembly of eastern Gondwana. Tectonophysics 362, 1–40.

Mercier, A., Debat, P., Saul, J., 1999. Exotic origin of the ruby deposits of the Mangari area in SE Kenya. Ore. Geol. Rev. 14 (2), 83–104.

Moecher, D., Essene, E.J., Anovitz, L.M., 1988. Calculation and application of clinopyroxene – garnet – plagioclase – quartz geobarometer. Contrib. Miner. Petrol. 100 (1), 92–106.

Möller, A., Mezger, K., Schenk, V., 1998. Crustal age domains and the evolution of continental crust in the Mozambique belt of Tanzania: combined Sm-Nd, Rb-Sr, and Pb-Pb isotopic evidence. J. Petrol. 39, 749–783.

Möller, A., Mezger, K., Schenk, V., 2000. U-Pb dating of metamorphic minerals; Pan-African metamorphism and prolonged slow cooling of high-pressure granulites in Tanzania, East Africa. Precambr. Res. 104, 123–146.

Muhongo, S., Tuisku, P., Mtoni, Y., 1999. Pan-African pressure-temperature evolution of the Merelani area in the Mozambique belt in Northeast Tanzania. J. Afr. Earth Sci. 29 (2), 353–365.

Muhongo, S., Kröner, A., Nemchin, A.A., 2001. Single zircon evaporation and SHRIMP ages for Granulite-Facies Rocks in the Mozambique Belt of Tanzania. J. Geol. 109, 171–189.

Pinna, P., Muhongo, S, Mcharo, B.A., Le Goff, E., Deschamps, Y., Ralay, F., Milesi, J.P., 2004. Geology and Mineral Map of Tanzania, scale 1:2,000,000. 20th Colloquium of African Geology – Orleans, France – 2–7 June, 2004, Abstracts volume, 337.

Shackelton, R., 1993. Tectonics of the lower crust : a view from the Usambara Mountains NE Tanzania. Struct. Geol. 15, 663–671.

Simonet C., 2000. Géologie des gisements de saphir et de rubis. L'exemple de la John Saul Ruby Mine, Mangare, Kenya. Doctoral thesis, université de Nantes, faculté des sciences et des techniques, 349 p.

Simonet, C., Fritsch, E., Lasnier, B., 2008. A classification of gem corundum deposits aimed towards gem exploration. Ore. Geol. Rev. 34, 127–133.

Sommer, H., Kröner, A., Muhongo, S., Wingate, M.T.D., 2003. Metamorphic petrology and zircon geochronology of high-grade rocks from the central Mozambique Belt of Tanzania: Crustal recycling of Archaean and Palaeoproterozoic material during the Pan-African orogeny. J. Metamorph. Geol. 21, 915–934.

Sommer, H., Kröner, A., Hauzenberger, C., Muhongo, S., 2005. Reworking of Archaean and Palaeoproterozoic crust in the Mozambique Belt of central Tanzania as documented by SHRIMP zircon geochronology. J. Afr. Earth Sci. 43 (4), 447–463.

Stern, R.J., 1994. Arc assembly and continental collision in the Neoproterozoic East African orogen: Implication for the consolidation of Gondwanaland. Annu. Rev. Earth Planet. Sci. 22, 319–351.